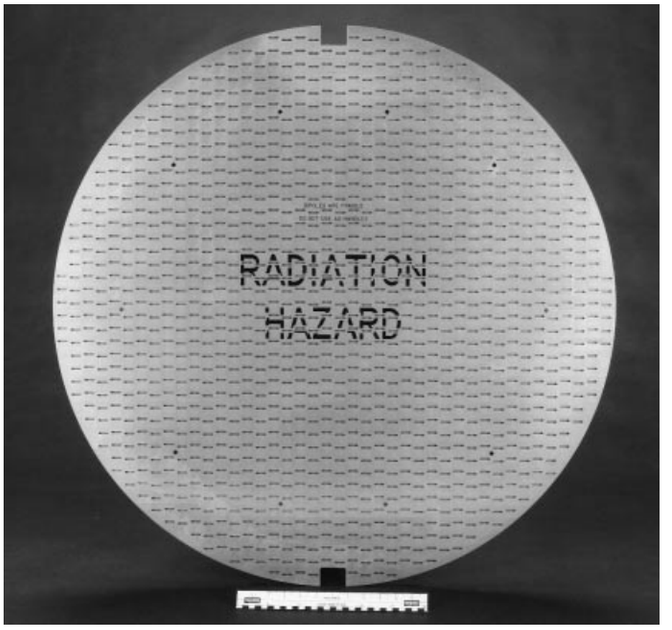

Figure 1. Waveguide slot array for an airborne radar application. (Courtesy of Raytheon Systems Co.)

WAVEGUIDE ANTENNAS

Waveguide antennas are useful for a variety of airborne, ground based, space, and missile applications in the microwave frequency band because they offer high radiating efficiency, a high degree of control over the radiation pattern, compact architecture, and low weight. The high radiating efficiency and compact architecture, namely, the small depth compared to a parabolic reflector antenna with equivalent gain, combine to optimize the use of the available aperture area. Accurate control of the radiation pattern allows designing arrays with a radiation pattern envelope tailored to the specific application. The low weight minimizes the impact on the installation and allows mounting the antenna on a mechanical gimbal assembly to scan the radiation pattern. A waveguide slot array designed to mount on a gimbal for an airborne radar application is shown in Fig. 1.

In waveguide slot arrays the radiating and transmission structures are inexorably intertwined, thus it is appropriate to treat the history of the waveguides together with that of slot radiators. In the 1930s, G. C. Southworth (1) at Bell Telephone Laboratories investigated electromagnetic propagation in hollow waveguides. Carson, Mead, and Schelkunoff performed the accompanying theoretical analysis (2). Independent work by Barrow of MIT (3) was published at about the same time (4). The analysis of waveguides and slot radiators in terms of transmission lines is also due to Schelkunoff (5). Another aspect of array work is the need for pattern synthesis. S. A. Schelkunoff's classic 1943 paper (6) and the subsequent C. L. Dolph (7) paper on the synthesis of equal sidelobe levels were used by T. T. Taylor (8) to achieve practical array designs. The major work on waveguide slot arrays during World War II was carried out in Canada at McGill University by W. H. Watson and his colleagues (9). The basis of their work included A. F. Stevenson's (10) analysis of the behavior of radiating slots in waveguides. Significant advances were made at the MIT Radiation Lab and are summarized in S. Silver's book (11). Further work was carried out by members of this group and others at Hughes Aircraft Co. in Culver City, CA (12). A. A. Oliner (13,14) and others refined Stevenson's theory at Polytechnic Institute of Brooklyn. R. S. Elliott and his students at UCLA, and numerous other researchers worked to further refine the design process.

The rectangular waveguide is the guide geometry used for most waveguide slot arrays because it provides a compact, low-loss transmission line which contributes to the high efficiencies achievable with these arrays. The basic radiating element, a single rectangular slot located in an infinite ground plane, is the complement to a dipole radiator (15) and, like the dipole, produces a broad radiation pattern. The radiating slot in the rectangular waveguide is realized in a variety of configurations, thus providing flexibility for the designer. The slot radiation characteristics are controlled by adjusting the slot location on the waveguide and the slot length and width.

An array of slots with a specified aperture distribution generates a highly directive or specially shaped radiation pattern. Arrays of slots are created by placing slot radiators in a waveguide to create a linear array and by joining a number of these waveguides with a power-divider network to create a planar array. Slots are used to couple energy between waveguides, and these coupling slots provide a compact way to realize the power-divider network. The closed-feed network eliminates the spillover loss suffered in horn-fed reflectors and other space-fed antennas. The aperture distribution is determined by the radiating slot characteristics and the power dividers in the feed network. The designer adjusts these pa-

rameters to achieve a high degree of control of the aperture distribution and thereby achieves a low-sidelobe or shaped-beam radiation pattern. The design process for these arrays is complex because of the need to accurately characterize the relationship between the slot geometry and performance and also because of interactions between the various elements of the array. The characteristics of the individual elements are derived from the interaction of the slot with the modes in the waveguide, and a simple lumped-circuit model is used to approximate the slot characteristics. The initial array design approach uses these lumped circuit elements to approximate array performance. The lumped-circuit model neglects interactions between the elements created by radiated and internal electromagnetic coupling. Refinement of the design to compensate for the interactions is done with experimental hardware or sophisticated electromagnetic simulation software.

WAVEGUIDE RADIATING SLOTS

A rectangular slot cut into a metallic ground plane radiates when an electric field is excited across the slot. The electric field distribution in the slot must meet the boundary condition that the tangential electric field at the slot boundary is zero. The lowest mode that meets the boundary conditions has a constant electric field directed across the width of the slot with a cosinusoidal distribution along the length of the slot:

$$E^{\mathrm{s}}(x,z) = \hat{x}\frac{V^{\mathrm{s}}}{w}\cos(\pi z/l) \text{ for } -w/2 < x < w/2, -l/2 < z < l/2 \tag{1}$$

where V^{s} is the peak voltage across the slot. The far-field radiation pattern of the slot located in an infinite ground plane is calculated by using Babinet's principle (15) (or image theory). For a slot located in the x–z plane, this results in a radiation pattern given by

$$\begin{aligned} E_\phi &= E_\phi(\theta,\phi)\frac{e^{-jkR}}{R} \\ E_\phi(\theta,\phi) &= \frac{-jV^{\mathrm{s}}k\sin\theta}{l}\frac{\cos(kl/2\cos\theta)}{(\pi/l)^2 - k^2\cos^2\theta} \end{aligned} \tag{2}$$

If the slot size is adjusted to the lowest resonance, the loss due to reactive energy is minimized, and the slot coupling is enhanced. At resonance, when the slot is assumed to be equal to one-half the free space wavelength, the radiation pattern becomes

$$E_\phi(\theta,\phi) = \frac{-jV^{\mathrm{s}}}{\pi}\frac{\cos(\pi/2\cos\theta)}{\sin\theta} \tag{3}$$

The directivity for a radiator measures the focusing effect of the radiator and is defined as the directivity relative to that for an isotropic radiator:

$$D(\theta,\phi) = \frac{4\pi P(\theta,\phi)}{\displaystyle\int_0^{2\pi}\int_0^{\pi} P(\theta,\phi)\sin\theta d\,\theta d\,\phi} \tag{4}$$

and the power is given by

$$P(\theta,\phi) = \frac{1}{2}\sqrt{\frac{\epsilon}{\mu}}|\mathbf{E}(\theta,\phi)|^2 \tag{5}$$

The gain of the element is given by the directivity minus any losses in the antenna. The directivity and gain are typically quoted in decibels. For a resonant slot, assuming that radiation occurs only above the ground plane, the peak directivity is 5.6 dB above that of an isotropic radiator.

Rectangular Waveguide Modes

The field in a waveguide slot is created by a displacement current caused by disruption of the currents generated on the waveguide walls by the energy in the waveguide modes. A metal-walled rectangular waveguide has a set of waveguide modes that satisfy the boundary conditions imposed on the fields by the metallic walls. These modes are classified into two types: the transverse electric (TE) which has only a magnetic field component in the direction of propagation and the transverse magnetic (TM) which has an electric field component only in the direction of propagation. The complete sets of field components for these modes for a lossless waveguide are as follows (16): for the $\mathrm{TE}_{\mathrm{mn}}$ modes,

$$\begin{aligned} H_z &= \cos\left(\frac{m\pi x}{a}\right)\cos\left(\frac{n\pi y}{b}\right)\, e^{-\gamma_{mn}z} \\ H_x &= -\frac{\gamma_{mn}}{j\omega\mu}E_y = \frac{m\pi\gamma_{mn}}{\kappa_{mn}^2 a}\sin\left(\frac{m\pi x}{a}\right)\cos\left(\frac{n\pi y}{b}\right)\, e^{-\gamma_{mn}z} \\ H_y &= \frac{\gamma_{mn}}{j\omega\mu}E_x = \frac{n\pi\gamma_{mn}}{\kappa_{mn}^2 b}\cos\left(\frac{m\pi x}{a}\right)\sin\left(\frac{n\pi y}{b}\right)\, e^{-\gamma_{mn}z} \\ \kappa^2 &= \left(\frac{m\pi}{a}\right)^2 + \left(\frac{n\pi}{b}\right)^2 \end{aligned} \tag{6}$$

and for the $\mathrm{TM}_{\mathrm{mn}}$ modes,

$$\begin{aligned} E_z &= \sin\left(\frac{m\pi x}{a}\right)\sin\left(\frac{n\pi y}{b}\right)\, e^{-\gamma_{mn}z} \\ E_x &= -\frac{\gamma_{mn}}{j\omega\mu}H_y = -\frac{m\pi\gamma_{mn}}{\kappa_{mn}^2 a}\cos\left(\frac{m\pi x}{a}\right)\sin\left(\frac{n\pi y}{b}\right)\, e^{-\gamma_{mn}z} \\ E_y &= \frac{-\gamma_{mn}}{j\omega\mu}H_x = \frac{n\pi\gamma_{mn}}{\kappa_{mn}^2 b}\sin\left(\frac{m\pi x}{a}\right)\cos\left(\frac{n\pi y}{b}\right)\, e^{-\gamma_{mn}z} \end{aligned} \tag{7}$$

The waveguide mode propagates unattenuated, except for ohmic losses, for frequencies where the propagation constant

$$\gamma_{mn} = \sqrt{\left(\frac{m\pi}{a}\right)^2 + \left(\frac{n\pi}{b}\right)^2 - k^2} \tag{8}$$

is imaginary. The wavelength at which this first occurs, the cutoff wavelength, is given by

$$\lambda = 2/\sqrt{(m/a)^2 + (n/b)^2} \tag{9}$$

For almost all applications it is desirable to operate with only a single propagating mode. The mode with the lowest cutoff frequency, the TE_{10} mode, is used. The guide dimensions are chosen to allow only this mode to propagate over the desired frequency range. The ohmic losses increase as the frequency approaches the cutoff frequency, therefore it is generally de-

sirable to operate at least 20% above the waveguide cutoff frequency. It is also preferable to operate a similar amount below the onset of the next propagating mode. The waveguide fields for the dominant TE_{10} mode are given by

$$\begin{aligned} H_z &= j\cos\left(\frac{\pi x}{a}\right) e^{\mp j\beta_{10}z} \\ H_x &= \mp\frac{\beta_{10}}{\pi/a}\sin\left(\frac{\pi x}{a}\right) e^{\mp j\beta_{10}z} \\ E_y &= \frac{\omega\mu_0}{\pi/a}\sin\left(\frac{\pi x}{a}\right) e^{\mp j\beta_{10}z} \end{aligned} \tag{10}$$

where the upper sign denotes a wave traveling in the $+z$-direction and the lower sign denotes a wave traveling in the $-z$-direction. The propagation constant for this mode is given by

$$\gamma_{10} = j\beta_{10} = j\sqrt{k^2 - \left(\frac{\pi}{a}\right)^2} \tag{11}$$

and the wavelength in the guide is given by

$$\lambda_g = \frac{\lambda}{\sqrt{1 - \left(\frac{\lambda}{2a}\right)^2}} \tag{12}$$

The relationship $\boldsymbol{J} = 1_n \times \boldsymbol{H}$ gives the electric currents flowing on the broadwall surface of the waveguide for this mode as

$$\begin{aligned} J_x &= j\cos\left(\frac{\pi x}{a}\right) e^{-j\beta_{10}z} \\ J_z &= \frac{-\beta_{10}}{\pi/a}\sin\left(\frac{\pi x}{a}\right) e^{-j\beta_{10}z} \end{aligned} \tag{13}$$

Waveguide Slot Radiation Mechanism

If slots are cut into the waveguide in locations where they interrupt the current flow, shown in Fig. 2, a displacement current is set up across the slot and radiation occurs. The amount of radiation is determined by the amount of current intercepted and is controlled by adjusting the slot position on the waveguide and its length and width. A variety of locations create slots with significant amounts of radiation. Slots are also made to radiate by introducing discontinuities into the waveguide, such as probes, wires, posts, and irises.

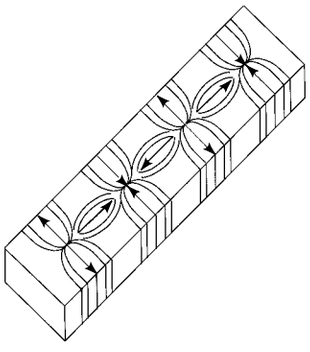

Figure 2. Rectangular waveguide current distribution for the TE_{10} mode.

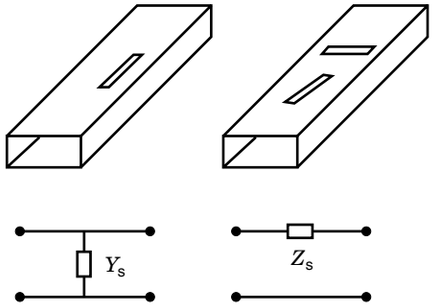

Figure 3. Waveguide radiating slots and their lumped-element circuit models: offset longitudinal shunt slot, and angled and transverse series slot.

The slot scatters energy in the waveguide in addition to radiating energy. The slot acts as an obstacle in the equivalent transmission line, and it is modeled as a lumped-circuit element in a two-wire transmission line (15). The lumped-circuit model has a resistive component representing the power lost to the radiated fields and a reactive component representing the stored energy. The backward and forward scattered waves for a slot in the waveguide wall are calculated from (10)

$$\begin{aligned} B_{10} &= \frac{1}{2S_a}\int_{\text{Slot}} (jE_tK_t + E_zK_z)e^{-j\beta_{10}z}\,dS \\ A_{10} &= \frac{1}{2S_a}\int_{\text{Slot}} (jE_tK_t - E_zK_z)e^{+j\beta_{10}z}\,dS \end{aligned} \tag{14}$$

where S_a is twice the Poynting energy flux for the dominant mode, $\boldsymbol{E}$ is the electric field in the slot, and $\boldsymbol{K}$ is the surface current density on the waveguide wall if the slot were not present. The scattering characteristics are used to compute the equivalent circuit characteristics and their dependence on the slot location and geometry. The slots are characterized by their location and orientation in the waveguide and by their equivalent circuit characteristics. Several slot geometries and their equivalent circuit models are shown in Fig. 3.

Waveguide Radiating-Slot Geometries

Offset Longitudinal Shunt Slot. A narrow slot located along the waveguide broadwall centerline does not radiate a significant amount of energy because it causes minimal disruption to the current flow on the waveguide walls. As the slot is offset from the waveguide centerline, it intercepts more of the waveguide currents, and the amount of power radiated becomes significant. The phase of the radiated field is reversed if the slot is located on the opposite side of the waveguide centerline. For an offset slot, it is a reasonable approximation to assume that the fields in the slot are symmetrical, and it can be shown that the scattering from the slot in the waveguide is also symmetrical. This symmetrical scattering corresponds to a shunt obstacle for the lumped-circuit model. The scattering for the slot is given by (17).

$$B_{10} = A_{10} = \frac{j2V^s(\pi/a)^2(\pi/l)}{\omega\mu_o ab\beta_{10}[(\pi/l)^2 - \beta_{10}^2]}\cos\left(\frac{\beta_{10}l}{2}\right)\sin\left(\frac{\pi x}{a}\right) \tag{15}$$

This assumes a narrow offset slot with only a E_x component that has the cosinusoidal distribution given in Eq. (1). This

can be related to the modes in a two-wire transmission line to calculate the conductance of the lumped circuit element:

$$\frac{Y}{G_0} = K_1 f(x,l)\frac{V^s}{V}$$

where

$$K_1 = \frac{2\pi}{ja}\sqrt{\frac{2}{kG_0\eta\beta_{10}ab}} \tag{16}$$

and

$$f(x,l) = \frac{(\pi/l)\cos(\beta_{10}l/2)}{(\pi/l)^2 - \beta_{10}^2}\sin(\pi x/a)$$

where x is the slot offset from the centerline and G_0 is the characteristic conductance of the guide. At resonance, when the slot length is one-half a free-space wavelength, the scattering coefficient is given by

$$B_{10} = \frac{j2V^s}{\omega\mu_0(\beta_{10}/k)ab}\cos\left(\frac{\pi\beta_{10}}{2k}\right)\sin\left(\frac{\pi x}{a}\right) \tag{17}$$

and the slot is represented by a shunt conductance. The conductance value is a function of the slot offset and the waveguide dimensions. The dependence of the conductance on the slot offset is given by (10,18)

$$\frac{G}{G_0} = g = g_1\sin^2\frac{\pi x}{a}$$
$$g_1 = 2.09\frac{\lambda_g}{\lambda}\frac{a}{b}\cos^2\left(\frac{\pi\lambda}{2\lambda_g}\right) \tag{18}$$

These equations are useful for understanding the slot characteristics but are not accurate enough for many design applications. The amount of radiation from the slot is controlled primarily by the offset and length as expressed previously but also depends on the slot width and the thickness of the wall in which the slot is cut. The slot resonant frequency must also be determined accurately. The slot is defined to be resonant when the phase of the scattered field is 180° out of phase with the incident wave. The resonant frequency occurs when the slot length is approximately one-half of a free-space wavelength, but the exact frequency is also a function of the slot offset, width, and thickness. The characteristics of the slot are determined more accurately by using an electromagnetic simulation technique, such as the method of moments (19), or by careful measurements. Figure 4 shows the variation of the slot conductance and resonant frequency as the offset and length are varied. The slot characteristics were calculated by using a computer simulation based on the method of moments formulation described in Khac (20), with slot thickness effects were added. The variation of the slot admittance normalized to the peak conductance values versus frequency relative to the resonant frequency for a slot in full height (2.3 cm × 1.0 cm) X-band (8 GHz to 12 GHz) waveguide is shown in Fig. 5. Away from the resonant frequency, the slot becomes reactive, and the radiation is reduced. The variation with frequency is relatively insensitive to the slot offset and length, so the curves are applicable over a wide range of offset and length

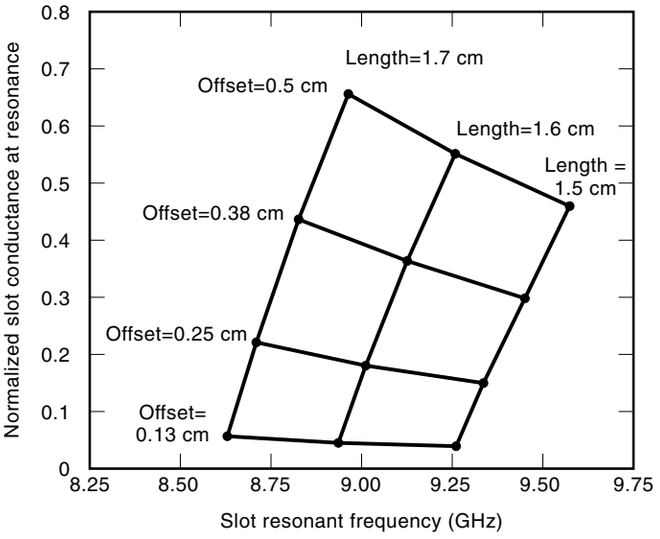

Figure 4. Offset shunt-slot resonant frequency and conductance for various slot lengths and offsets.

values. If the slot offset is large or the waveguide height is reduced considerably, $b < a/4$, the fields in the slot are less symmetrical, and the slot behaves less like a pure shunt element (21). For these cases a more complicated circuit model is required, or the scattering matrix description should be used instead of a lumped-circuit model.

Broadwall Series Slots. A slot cut transversely across the waveguide broadwall radiates when centered in the waveguide, and the amount of radiation is controlled by adjusting the offset. For this element the forward scattered field is opposite in sign to that of the backscattered field, so this slot is

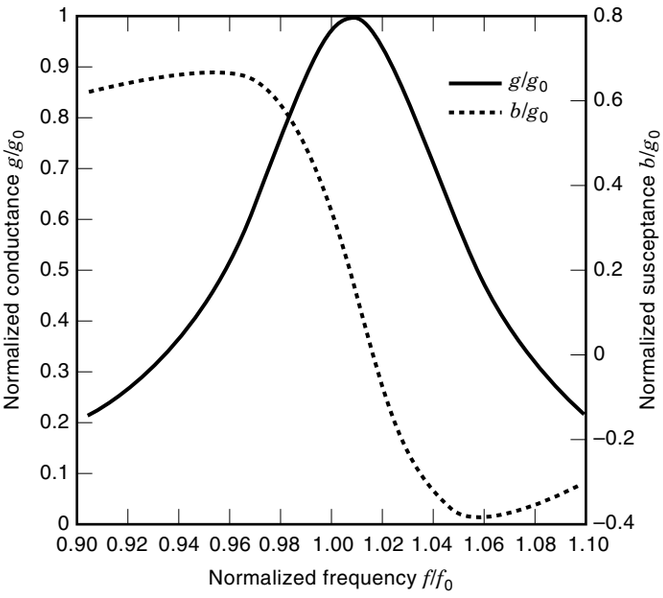

Figure 5. Variation of normalized conductance and admittance for an offset-shunt slot relative to the resonant frequency.

modeled as a series element. The normalized series resistance for this element is given by

$$\frac{R}{R_0} = r = r_1 \cos^2\left(\frac{\pi x_1}{2}\right)$$
$$r_1 = 0.523\left(\frac{\lambda_g}{\lambda}\right)^3 \frac{\lambda^2}{ab}\cos^2\left(\frac{\pi\lambda}{4a}\right) \tag{19}$$

The maximum coupling for this element occurs when the slot is centered. This slot has a high coupling value, but the range of coupling attainable is limited because the slot length restricts the range of offsets, and the slot is confined to the broadwall.

A slot located along the waveguide centerline also radiates when rotated at an angle relative to the centerline. The forward scattering from this element is opposite in phase to that of the backscattered field, and hence it is modeled as a series lumped element. The amount of power coupled is controlled primarily by the slot angle and is adjustable over a wide range of coupling values.

$$\frac{R}{R_0} = r = 0.131\left(\frac{\lambda}{\lambda_g}\right)\frac{\lambda^2}{ab}\left[I(\theta)\sin\theta + \frac{\lambda_g}{2a}J(\theta)\cos\theta\right]^2$$
$$\left.\begin{matrix} I(\theta) \\ J(\theta) \end{matrix}\right\} = \frac{\cos\left(\frac{\pi\xi}{2}\right)}{1-\xi^2} \pm \frac{\cos\left(\frac{\pi\eta}{2}\right)}{1-\eta^2} \tag{20}$$
$$\left.\begin{matrix} \xi \\ \eta \end{matrix}\right\} = \frac{\lambda}{\lambda_g}\cos\theta \mp \frac{\lambda}{2a}\sin\theta$$

The resonant frequency for this slot is relatively insensitive to the slot angle. The polarization characteristics of the slot rotate with the slot orientation and generate a cross-polarization component which limits its usefulness in systems where polarization purity is required.

Narrow-Wall and End-Wall Slots. Transverse angle slots located in the narrow wall of the waveguide are also used as radiating elements. The height of the narrow wall is typically less than the half free-space wavelength required for a resonant slot. So to achieve resonance, the ends of the slot are extended into the broadwall. The coupling is controlled by the slot angle and the depth to which the slot extends into the broadwall. This slot exhibits a cross-polarization component that varies with the slot angle. This geometry is difficult to model accurately.

Slots located in the shorted end of a waveguide are used for phased-array applications. The slot radiation is created by the disruption of the currents in the terminating short of the waveguide. For most phased-array applications, the slot characteristics are chosen to provide the best match in the array environment, and the power to the slot is controlled by the feed network. Open-ended waveguides are frequently used for scanned-array applications.

WAVEGUIDE COUPLING SLOTS

In addition to their function as radiating elements, slots are also used to couple energy between waveguides. The electric field excited in the slot by the incident mode at the input port excites fields in the coupled waveguide. In conjunction with linear radiating slot arrays, the coupling slots provide the building blocks for the planar slot array. The slot configurations described for the radiating elements are also applied as coupling elements. Coupling between the broadwalls is useful to create arrays with minimal depth, and coupling is achieved with the waveguides parallel or perpendicular to each other.

The coupling slots can be modeled by using lumped-circuit elements. For these elements a transformer between two sets of two-wire lines models the coupling characteristics, and a reactive element models the stored energy in the slot. The slot-coupling ratio determines the turns ratio for the transformer model. The slot is described in terms of its lumped-element characteristics in each of the lines. The element may be a series–series, shunt–shunt, or shunt–series element depending on its orientation in the two waveguides.

Coupling-Slot Characterization

The characteristics of these elements are determined by a method similar to that for the radiating elements. The forward and backward scattering components are the same as those for the radiating slot given in Eq. (14). Now they are applied in both the input and coupled guides to give the backscattered, forward-scattered and coupled fields. The coupling coefficient between the waveguides is a function of the slot characteristics in the two waveguides and the characteristic impedances of the two guides. The power balance requirement is applied to the junction to show that the coupling coefficient can be calculated from the ratio of the scattered fields and characteristic impedances in the two guides. The scattered-field terms are the same as those derived for the radiating slot except for the value of the coefficient of the field in the slot. For the coupling slot, the ratio of the scattered fields in the two guides is independent of the value of the coefficient, so it need not be determined. The coupling ratio for the slot is given by (22)

$$M = \frac{a_1 b_1 Y_1 |B_1|^2}{a_2 b_2 Y_2 |B_2|^2} \tag{21}$$

where Y_1 and Y_2 are the characteristic impedances in the input and coupling guides, respectively, and B_1 and B_2 are the backscattered fields in the two guides. The value of $1/\sqrt{M}$ gives the turns ratio for the transformer in the lumped-circuit model.

Coupling-Slot Geometries

The series–series angle slot is a convenient element for broadwall coupling between transverse waveguides because the coupling is controlled by adjusting the slot angle without changing the relative locations of the waveguides and a wide range of coupling values is attainable. This slot and its equivalent circuit model are shown in Fig. 6. The coupling value for this element at resonance, assuming a narrow rectangular slot with zero thickness, is given by

$$M = \frac{a_2 b_2 \lambda_{g_2}}{a_1 b_1 \lambda_{g_1}}\left[\frac{I_1(\theta)\sin\theta + \frac{\lambda_{g_1}}{2a_1}J_1(\theta)\cos\theta}{I_2(\theta)\sin\theta + \frac{\lambda_{g_2}}{2a_2}J_2(\theta)\cos\theta}\right]^2 \tag{22}$$

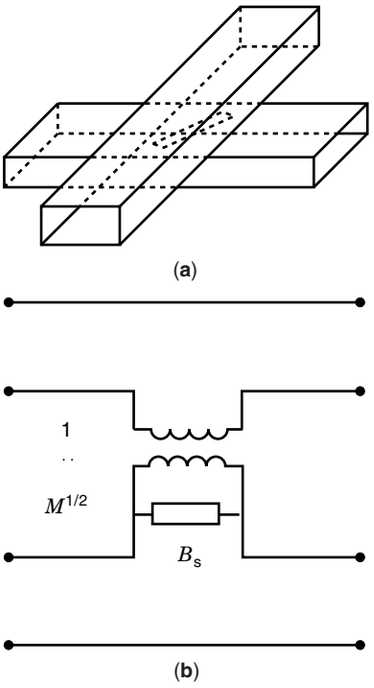

Figure 6. Series–series angle slot coupling element and its lumped-element circuit model.

where the expressions in the equation are the same as those defined in Eq. (20) for the angled radiating slot. The transverse series–series slot, which is the limiting case for the angled series–series slot, provides large coupling values between the guides.

The offset shunt–series coupling slot provides coupling between transverse waveguides. The slot is oriented as an offset shunt slot in one waveguide and a transverse series slot in the other. The coupling values are adjusted by changing the slot offset which is equivalent to moving the location of the shunt waveguide relative to the slot. The coupling value for this slot at resonance is given by

$$M = \frac{1}{4}\frac{a_2 b_2 \lambda_{g_1}\lambda_{g_2}}{a_1^3 b_1}\left[\frac{1-(l/a_2)^2}{1-(2l/\lambda_{g_1})^2}\right]^2 \frac{\cos^2(\beta_1 l/2)}{\cos^2(\pi l/2a_2)}\frac{\sin^2(\pi x_1/a_1)}{\cos^2(\pi x_2/a_2)} \tag{23}$$

where waveguide 1 contains the shunt-slot orientation.

These approximate values for the slot coupling depend on the accuracy of the assumption made for the field in the slot and neglect effects, such as slot thickness and the reactive component of the slot, as the frequency departs form the resonant frequency. More accurate models for the slot are derived by the method of moments (23). Computer simulation tools based on the finite-element method (24) are also suitable for modeling coupling slots because they operate in a closed structure. This differs from the radiating slot case which does not lend itself well to this type of model because the problem is unbounded.

LINEAR SLOT ARRAYS

A linear array of slots serves alone as an antenna or as a building block for a planar array. The far-field radiation pattern for a linear array of N elements located along the z-axis is given by

$$S(\phi,\theta) = A(\phi,\theta)\sum_{n=1}^{N} V_n e^{jkz_n\cos\theta} \tag{24}$$

The $A(\phi, \Phi)$ term is the radiation pattern of a single radiating element, which is assumed to be the same for all elements in the array. The element pattern is similar to that given in Eq. (2), but it is modified by the array environment. The summation term represents the array factor where V_n are the excitation values and z_n are the element locations. The excitation values of the elements are chosen to generate a specified array radiation pattern. Slot-radiating elements allow controlling the excitations to achieve the desired pattern characteristics.

Linear arrays are divided into two categories: the standing-wave (or resonant array) and the traveling-wave array (or nonresonant array). The antenna and system performance requirements dictate the choice between the two configurations. In the standing-wave array, the slot locations are chosen to maximize the coupling at the design frequency, and the waveguide is terminated with a short circuit. This creates an efficient antenna, but the bandwidth is limited. In the traveling-wave array, the slot spacings are nonresonant, and the waveguide is terminated with an absorptive load. The traveling-wave array operates over a larger frequency bandwidth than the standing-wave array, but the power absorbed by the load reduces the radiating efficiency. It is difficult to generate a beam perpendicular to the guide with the traveling-wave array, and it also exhibits beam scan with frequency.

Standing-Wave Arrays

For the resonant array, standing-wave fields are created in the waveguide by terminating the waveguide with a metal wall to create a short circuit. The slot locations relative to the short circuit are chosen to maximize the array radiation coupling. For series elements, such as the angled series slot, the slots are located multiples of a half guide wavelength from the short circuit. For shunt elements, such as the offset-shunt slot, the maximum coupling locations are multiples of a half guide wavelength from an open circuit which is achieved by locating a short circuit at one-quarter guide wavelength from the nearest slot. For broadside operation the slots are located in the guide to achieve a uniform phase distribution. A uniform phase distribution is achieved by locating the slots at one guide-wavelength intervals. However this results in an array spacing greater than one free-space wavelength which creates multiple main beams and reduces the antenna gain and performance. The spacing can be reduced to one-half guide-wavelength intervals by alternating the slot offsets to compensate for the 180° phase reversal in the guide.

Circuit Model for Resonant Linear Array. A circuit model of the array provides a good starting point for predicting the array performance and for determining the slot dimensions. The array is modeled by using the lumped-circuit elements for the individual slots, transmission line sections representing the waveguide sections, and a short circuit termination. An offset-shunt-slot linear array and its circuit model are

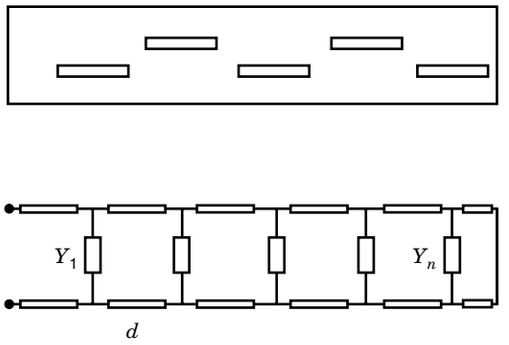

Figure 7. Waveguide linear array of offset longitudinal shunt-slot radiators and its transmission line circuit model.

shown in Fig. 7. The transmission matrix is defined as (25)

$$\begin{bmatrix} V_i \\ I_i \end{bmatrix} = \begin{bmatrix} A & B \\ C & D \end{bmatrix} \begin{bmatrix} V_{i+1} \\ I_{i+1} \end{bmatrix} \tag{25}$$

A section of transmission line of length d with a propagation constant β and a characteristic impedance Z_0 has a transmission matrix

$$\begin{bmatrix} \cos(\beta d) & jZ_0 \sin(\beta d) \\ \dfrac{j}{Z_0} \sin(\beta d) & \cos(\beta d) \end{bmatrix} \tag{26}$$

The transmission matrices for the shunt element with admittance Y and series element with impedance Z are

$$\begin{bmatrix} 1 & 0 \\ \mathrm{Y} & 1 \end{bmatrix} \text{ and } \begin{bmatrix} 1 & Z \\ 0 & 1 \end{bmatrix} \tag{27}$$

To achieve a satisfactory design, the coupling values for the individual slots must be chosen so that the reflection coefficient at the array input achieves the required value and so that the relative coupling from the slots generates the desired radiated phase and amplitude distribution for the array. The input match to the array and its variation with frequency is modeled by cascading the transmission matrices for the slots and the waveguide sections. At the array resonant frequency the normalized input conductance or resistance for an array of N shunt or series slots reduces to

$$\frac{Y_i}{Y_0} = \sum_{n=1}^{N} \frac{Y_n}{Y_0}$$

or

$$\frac{Z_i}{Z_0} = \sum_{n=1}^{N} \frac{Z_n}{Z_0} \tag{28}$$

The input reflection coefficient is given by

$$\Gamma_i = \frac{1 - Y_i/Y_0}{1 + Y_i/Y_0} = \frac{Z_i/Z_0 - 1}{Z_i/Z_0 + 1} \tag{29}$$

To achieve an input match for an end-fed standing-wave array, the slot parameters should be chosen so that the slot conductances or impedances sum to one. The slot conductances must also be selected to obtain the amplitude distribution required to achieve the desired radiation pattern. If the slots are all assumed to be resonant and the desired distribution is all equiphase, the ratios of the slot conductances are proportional to the relative slot radiated powers. This gives a set of N equations that can be solved to give the required slot conductances for a shunt-slot array:

$$\frac{G_i}{G_0} = \frac{G_1}{G_0} \sum_{n=1}^{N} \frac{P_n^r}{P_1^r}$$

$$\frac{G_n}{G_0} = \frac{G_m}{G_0} \frac{P_n^r}{P_m^r}$$

The offset-shunt slot is a commonly used element for linear arrays. It offers a wide range of conductance values and linear polarization. The slot offsets and length can be computed using the equations for the offset shunt slot given earlier, or interpolated from a graph, such as Fig. 4.

Array Mutual-Coupling Effects. The simple circuit model design is useful for understanding the slot array or for determining a set of initial design values, but it is not accurate enough for most applications. The assumption was made that the slots in the array have the characteristics of an isolated slot. In the array environment the slots are affected by the presence of the other slots, and slots at the edge of the array exhibit behavior that differs significantly from that of slots in the center of the array. If neglected, these effects result in an array where the input reflection coefficient and radiation pattern depart significantly from the desired values. The characteristics of the isolated slot were determined by using a single source of excitation for the slot: the incident waveguide mode. Multiple sources in the array environment excite the slot: the incident field, the fields scattered in the waveguide by the other slots in the guide, and the radiated fields from all the other slots. The characteristics for each slot are influenced by all the other slots in the array to some extent, so a slot's configuration cannot be determined independently. A series of simultaneous equations is required to perform the array design. Elliott (17) has developed a series of design equations that account for the internal and external mutual coupling effects:

$$\frac{Y_p^a/G_0}{Y_n^a/G_0} = \frac{f_p}{f_n} \frac{V_p^s}{V_n^s} \frac{V_n}{V_p} \tag{30}$$

$$\frac{Y_n^a}{G_0} = \frac{2f_n^2}{\dfrac{2f_n^2}{Y/G_0} + j(\beta_{10}/k)(k_0 b)(a/\lambda)^3 \displaystyle\sum_{m=1}^{N'} \frac{V_m^s}{V_n^s} g_{mn}}$$

$$f_n(x_n, l_n) = \frac{(\pi/l)\cos(\beta_{10} l_n)}{(\pi/l_n)^2 - \beta_{10}^2} \sin\left(\frac{\pi x_n}{a}\right)$$

$$g_{mn}(x_n, l_n, x_m, l_m) = \int_{-l_m/2}^{l_m/2} \cos(\pi \zeta_m'/l_m) \int_{-l_n/2}^{l_n/2} \cos(\pi \zeta_n'/l_n) \left[\frac{\partial^2}{\partial \zeta_n^2} + k_0^2\right] \frac{e^{-jk_0 R}}{R} d\zeta_n' \zeta_m' \tag{31}$$

The Y_n^a/G_0 are the active slot admittances in the array environment, the V_n^s, V_n are the slot and the waveguide mode voltages, and the g_{mn} terms represent the external mutual-coupling effects between the slots. The set of equations is applied iteratively along with the equation for the required input impedance to determine the slot offsets and lengths. These equations assume an ideal cosinusoidal distribution in a narrow slot, and may not be accurate enough for some applications. A more thorough analysis, where the field distribution in the slots are unknowns which must be determined, provides a more accurate model of the impact of element mutual coupling on array performance (26). The computational requirements for a rigorous analysis may limit the size of the array for which it is applicable. A good approximation to the final design should be found first by using an approximate method to reduce the number of iterations required.

Variation of Performance with Frequency. The design achieves the desired input match at the design frequency, but the input match of the linear array degrades as the frequency moves away from resonance. This effect is modeled using the transmission matrices by adjusting the propagation constant in the transmission line sections and including the variation of the slot admittance with frequency. The bandwidth is generally defined as the frequency range over which the input reflection coefficient remains below a specified level. The bandwidth is determined primarily by the number of elements in the array, and it degrades as the number of elements in the array increases. Watson (9) derived an approximate expression for the variation of the input reflection coefficient which neglects the multiple reflections:

$$\Gamma = \frac{2 - \sum_{n=1}^{N} Y_n/Y_0 - e^{j2N\beta d} \sum_{n=1}^{N} Y_n/Y_0 e^{-j2n\beta d}}{\left(2 + \sum_{n=1}^{N} Y_n/Y_0\right) e^{j2N\beta d} + \sum_{n=1}^{N} Y_n/Y_0 e^{j2n\beta d}} \tag{32}$$

The array excitations also change away from the center frequency because the slot locations relative to the standing wave in the guide are no longer optimum and the slot radiation characteristics also exhibit frequency variation. This causes pattern degradation and main-beam distortion. The effects are modeled by using the circuit model to determine the slot excitations and computing the far-field pattern generated by these excitations.

Traveling-Wave (Nonresonant) Arrays

For the nonresonant array, the array distribution is generated by progressively coupling energy from the waveguide mode as it travels down the guide. The element spacings are chosen to be nonresonant, and the waveguide is terminated with a matched load. The design process differs from that of the standing-wave array because the reflections from the slots do not add coherently at the input. The input reflection is controlled by the destructive interference due to the nonresonant spacing, and the reflection coefficients of the individual elements are kept small to minimize the reflection. The traveling-array input-match bandwidth does not decrease as the array size increases, unlike that of the resonant array. The resonant slot spacing case for a broadside beam is avoided because the summation of the individual reflections creates a large reflection. The traveling wave generates a linear phase slope across the aperture which corresponds to a scanned beam with the beam pointing direction given by (27)

$$\cos\theta_0 = \lambda/\lambda_g - \lambda/2d \tag{33}$$

for an array with alternating slot offsets. The beam scans with frequency due to the change in the guide wavelength. This frequency-scanning effect is often exploited by making the waveguide path length between the slots greater than the array spacing to enhance the amount of scan for a given frequency change (28). The beam position for this case is given by

$$\cos\theta_0 = d_g\lambda/d\lambda_g - \lambda/2d \tag{34}$$

Circuit Model for Nonresonant Arrays. The circuit model for the traveling-wave array is similar to that used for the resonant array, but a matched-load termination replaces the terminating short, and the line lengths are adjusted to reflect the nonresonant spacing. The initial design is simplified by assuming that the scattering from each slot is small, and hence multiple reflections are neglected. With this assumption and a perfect load termination, the reflection coefficient at the waveguide input is given by

$$\Gamma_i = \sum_{n=1}^{N} \rho_n e^{-j2n\beta d} \tag{35}$$

where the reflection coefficient for a resonant slot

$$\rho_n = \frac{-2G/G_0}{2 + G/G_0} \tag{36}$$

Neglecting the slot reflections, the ratios of the slot radiated powers for a traveling-wave array of resonant shunt elements are given by

$$\frac{P_n^r}{P_1^r} = \frac{G_n/G_0}{G_1/G_0} \prod_{i=1}^{n-1} \left(1 - \frac{G_i}{G_0}\right) \tag{37}$$

where the product term gives the decrease in the power along the guide caused by radiated energy. The ratio of the power remaining after the final element is absorbed in the load termination relative to the input power is given by

$$\frac{P_l}{P_i} = \prod_{n=1}^{N} \left(1 - \frac{G_n}{G_0}\right) \tag{38}$$

If the waveguide loss is significant, the attenuation factor $e^{-\alpha z}$ should be included in the power calculation. The initial design process requires solving these equations to achieve both the desired amplitude distribution and an acceptable value for the power lost to the load. For the traveling-wave array it is advantageous to have a longer array because this reduces the amount of power which must be absorbed in the load termination. The range of coupling values available for the radiating elements also affects the amount of power which will be lost in the load. The circuit models can be cascaded to account for the multiple reflections and frequency effects. The

design process for the array including mutual coupling effects is similar to that for the resonant array. However, the variation of the mode voltage along the array must be included in the model (29).

WAVEGUIDE PLANAR ARRAY

The waveguide planar array is constructed by joining a number of linear arrays via a feed network. The planar aperture provides the area required to achieve high gain which is a critical parameter for most designs as it determines the effective range of system operations. The rectangular waveguide exhibits low loss values over a wide range of frequencies (up to the millimeter wave band) which makes the waveguide slot array desirable for high-gain applications. The sidelobe distribution is also important for many applications as high sidelobes may result in unwanted interference between adjacent installations or false returns off scatterers located in the sidelobe region. For the planar-slot array, the aperture distribution is achieved by controlling the characteristics of the individual radiating elements and the coupling characteristics of the feed network. The ability to accurately control the excitation across the aperture allows the designer to set the radiation pattern sidelobes.

Planar-Array Far-Field Patterns

The equation to compute the far-field pattern of a planar array located in the x–y plane is

$$S(\theta,\phi) = A(\theta,\phi)\sum_{m=1}^{M}\sum_{n=1}^{N} V_{mn} e^{jk(x_{mn}\sin\theta\cos\phi + y_{mn}\sin\theta\sin\phi)} \quad (39)$$

The array elements are assumed to have identical element patterns which are similar to Eq. (2) with the appropriate coordinate transformation to match the element orientation. The array factor is given by the summation term where V_{mn} is the excitation of each element. If the array elements are on a rectangular grid, the equation simplifies to

$$S(\theta,\phi) = A(\theta,\phi)\sum_{m=1}^{M}\sum_{n=1}^{N} V_{mn} e^{jk(md_x\sin\theta\cos\phi + nd_y\sin\theta\cos\phi)} \quad (40)$$

This formulation is in the form of a Fourier transform, and with appropriate manipulations fast Fourier transform (30) computer routines are used to reduce computation time greatly. For a rectangular, separable array, the distribution is chosen to be of the form

$$V_{mn} = V_m V_n$$

Now the resulting planar-array equation is the product of the two linear-array distributions. This results in a dramatic reduction in computation time:

$$S(\theta,\phi) = A(\theta,\phi)\sum_{m=1}^{M} V_m e^{jkmd_x\sin\theta\phi}\sum_{n=1}^{N} V_n e^{jknd_y\sin\theta\sin\phi} \quad (41)$$

For arrays with separable distributions, the desired linear-array distributions are selected, and then the products are used to determine the individual element distributions. The cardinal plane patterns of the array match the linear-array patterns, and the intercardinal planes have sidelobes which are the product of the two linear-array distributions. For circular apertures, there are a variety of circular distributions available which are sampled to generate the array distribution (31). More complex distributions are synthesized for specific applications. The planar-array directivity is computed by using the array far-field pattern in the directivity expression, Eq. (4). The directivity is reduced by the losses in the antenna system to determine the array gain.

Resonant Planar-Array Design

A common architecture for a resonant planar array, shown in Fig. 8, uses broadwall offset-shunt slots as the radiating elements. The linear arrays are attached along the sidewalls, and common sidewalls are used to reduce the weight. Different lengths are used for the linear arrays to fit the array within a specified area. Power is fed to the individual linear arrays via a waveguide network beneath the radiating aperture. A compact feed network is formed with a linear array of broadwall coupling slots to distribute power to the radiating waveguides. Angled series–series slots provide a convenient coupling mechanism because the power to each linear array is controlled by adjusting the slot angle. Offset shunt–series slots are also used as coupling elements, but they have the disadvantage that the linear arrays must be offset to maintain the proper feed point and compensate for the staggered offsets of the coupling slot.

The radiating slots and feed network are designed together to provide the desired input match and to achieve the aperture radiating distribution. The design values for the radiating slots and the coupling slots must be chosen together to meet the performance goals as the input impedance and the slot radiation are functions of both the radiating slot values and the coupling values of slots in the feed waveguide. The array spacings to achieve resonance in both the radiating and feed planes are related because the radiating guide width determines the spacing in the feed plane. The spacings and the waveguide dimensions must be chosen as a set to achieve the correct resonant frequency in each plane of the array.

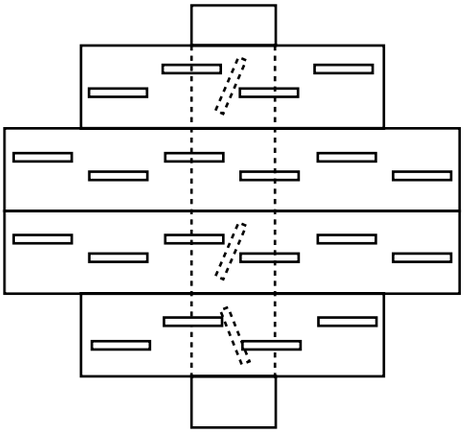

Figure 8. Waveguide planar array with offset longitudinal shunt-slot radiators and series–series angle-slot coupling elements.

Planar-Array Circuit Models. The lumped-circuit models used for the linear-array design combine with the coupling-slot models to provide a simple model for the planar array. The impedance at resonance of a series–series slot coupling to a linear array of M radiating slots is given by

$$R_n/R_0 = \frac{1}{M_n} \sum_{m=1}^{M(n)} G_{mn}/G_0 \tag{42}$$

The coupling elements form a linear array of N slots in the feed waveguide with an input impedance at resonance of

$$Z_i/Z_0 = \sum_{n=1}^{N} \frac{1}{M_n} \sum_{m=1}^{M(n)} G_{mn}/G_0 \tag{43}$$

The ratios of the slot conductance and coupling values must be chosen to provide the correct ratios for the radiating-slot voltages. The slot conductance values within each radiating guide are given by

$$G_{mn} = G_{1n} \frac{P^r_{mn}}{P^r_{1n}} \tag{44}$$

and the coupling ratio for each series–series slot is given by

$$M_n = M_1 \frac{\sum_{m=1}^{M(n)} G_{mn}/G_0 \sum_{m=1}^{M(1)} P^r_{m1}}{\sum_{m=1}^{M(1)} G_{m1}/G_0 \sum_{m=1}^{M(n)} P^r_{mn}} \tag{45}$$

The values for the G_{1n} and M_1 must be chosen to create the desired input impedance value. For compactness and improved bandwidth characteristics, it may be desirable to feed the array at the center of the feed waveguide using an additional feed layer with a coupling slot. For a shunt–series coupling element where the waveguide terminated by a short at one-quarter guide wavelength, the input admittance to the array is given by

$$Y_i = \frac{Z'}{\mathscr{M}_0} \tag{46}$$

where Z' is the impedance in the feed waveguide and $\mathscr{M}_0$ is the input slot coupling ratio. The values for the series–series coupling slots must be chosen to account for the power division between the elements to each side of the input slot.

Mutual-Coupling Effects. As in the linear array, the simple circuit model neglects effects, such as mutual coupling between the slots, that perturb the performance. The mutual-coupling effects between the radiating elements are handled as described for the linear array with a separate input admittance requirement for each radiating waveguide. The external mutual-coupling effects are generally more significant in the E-plane of the slots than in the H-plane. Additional coupling mechanisms which impact the array performance include coupling-slot interaction with the radiating slots and with the other coupling slots in the feed guide. The radiating slots closest to the coupling slots in each guide are significantly affected by these interactions. These interactions are modeled by the method of moments (32).

Large Resonant Arrays. The array bandwidth decreases as the size increases because of the increased number of elements in the radiating and feed linear arrays. To avoid the bandwidth reduction for a large array, the array is subdivided into a number of subarrays or modules with shorter radiating and feed arrays. The array power is distributed to the individual modules via a feed network made up of a series of waveguide power dividers. The configurations of the modules are dictated by the required array bandwidth, the available aperture area, and the packaging limitations for the feed network. It is desirable to minimize the modular size to improve the array bandwidth, but this requires more modules and complicates the feed network. Dividing the array into subarrays is fairly straightforward for rectangular arrays. The choice of modular layouts is more complex for arrays with elliptical or irregular boundaries. The available range of coupling values for the slots and the feed network limits the choice of modular configurations. Systems requirements, such as the need to provide both sum and difference patterns which necessitates dividing the array into equal quadrants, also determine the available configurations.

A typical configuration for a resonant planar array is built up of several modules with offset-shunt radiating slots and angled series–series coupling slots. Offset-shunt series slots are used to couple power from a waveguide corporate feed network made up of reactive H-plane waveguide three-port power dividers. For an array with difference pattern requirements, the power is distributed to the quadrants of the array by a network of waveguide magic-tee four-port power dividers. This architecture provides some inherent mechanical advantages due to the boxlike structure of the radiating aperture, and, depending on the array size, is packaged so that the depth of the array is as small as three times the waveguide b dimensions. Numerous other variations of array architecture are also used.

To begin the design of an array of this type, the desired gain and sidelobe performance and frequency bandwidth must be specified. The size of the array is driven by the array gain. The area is chosen so that the area directivity minus the taper loss, all losses in the aperture and feed networks, and any of the return loss at the array input meets the required gain value with some margin. Because of variations the required aperture distribution is selected to meet the sidelobe requirements with some margin. The array slot spacings are chosen to meet the frequency requirements and make the most effective use of the available area. The aperture distribution is discretized to give the required value at each slot. Then the array is subdivided into modules whose size is based on the required frequency bandwidth. The design of individual modules is similar to that described previously with the additional complication that now the external mutual coupling includes both the slots within the module and all slots in the other modules.

The feed network is a multiport power-dividing network with an output port for each module. The relative power to each port is calculated by summing the specified powers of the slots in each module. For most applications a corporate feed structure with equal path lengths to each module is required to meet the bandwidth requirements. A reactive H-plane tee in a rectangular waveguide provides a low-loss, low-profile power-dividing network. The individual tees are matched, and the power splits are controlled by adjusting in-

ductive-tuning irises at the tee input and the length and position of a septum on the back wall of the tee. The performance of the reactive-feed network is sensitive to the loads placed on the feed by the modules. To reduce this sensitivity and provide broader band performance, matched power dividers are used though they have higher loss and larger sizes.

Frequency and Power-Handling Effects. As the operating frequency of a resonant array moves away from the design frequency, the input match degrades and the pattern performance suffers. For arrays whose radiating guide and feed waveguides are fed near or at their centers, the amplitude and phase of elements at the ends of the guide diverge from those near the center. For a single module this broadens the main beam and increases the sidelobe level. For an array of modules, this creates an error across the array with a period equal to the modular spacing which creates error lobes in the far-field pattern and reduces the array directivity. These effects are modeled by using a circuit model for the modules and feed network.

The amount of power that the array is required to handle also influences the design. The waveguide power-handling capability is reduced as the waveguide b dimension is decreased, so for high-power applications full height waveguide should be used. For arrays which must operate at high altitudes, the waveguides are pressurized. Care should be taken to avoid any obstacles which protrude into the guide in the b dimension and mismatches should be minimized to reduce the standing-wave effect. The amount of power is reduced as it divides through the feed network and subarrays, so the power-handing problem is less severe at the aperture.

Nonresonant Planar Arrays

The traveling-wave planar array is created by joining a set a linear, traveling-wave arrays with a feed network. The sidewall edge-slot array is frequently chosen, particularly for applications where the array is scanned in the feed plane, because the linear arrays can be packed closely together. The radiating arrays are designed similarly to the linear array, but mutual coupling between the linear arrays must be taken into account. It is generally preferable not to subdivide the array and to end feed the radiating aperture to minimize the power lost to the loads. The feed network can be traveling wave or standing wave depending on the application. A linear array of coupling slots provides a compact feed network for many applications. Where beam squint in the feed plane is not desired, a corporate feed network of waveguide power dividers is used.

Effects of Manufacturing Variations

Array performance is influenced by how accurately the design is realized in manufacturing. For arrays with stringent sidelobe requirements, the effects of manufacturing deviations from the design values significantly alter the performance, and the deviations must be carefully controlled. The potential impacts of the manufacturing process should be accounted for in the design. Where possible, the design values should be chosen to minimize sensitivity to the variations. The acceptable limits for process variations should be set on the basis of acceptable performance limits; the processes should be chosen for compatibility with these limits. The relative locations of the features and the geometry of the individual features must be controlled. The potential cost impacts of overly tight tolerances must be weighed against the performance impacts. The operating frequency of the array is a major factor in the allowable tolerances and hence the preferred manufacturing technique. Typical manufacturing processes for slot arrays include machined metal assemblies joined either by brazing or bonding, stamped or punched slots, etched slots on metal clad dielectric, molded metallized plastic assemblies, or cast parts.

For slots manufactured by conventional machining techniques, it is more convenient and cost effective to machine the slots with a rounded end that matches the diameter of the endmill rather than create a true rectangular slot. For narrow slots, the main effect of the rounded end is a change in the slot resonant frequency. The effect is modeled and compensated for by assuming that a rounded end slot has the same resonant frequency as a square-ended slot of equal area (14).

For large arrays, errors that are randomly distributed across the array face result primarily in increased average sidelobe level and a decreased array gain. The effects of these errors are estimated by statistical techniques (33,34) or by a Monte Carlo simulation of the array pattern. The variation in the element excitation must be estimated from the tolerances on the element features, and then these values are used to estimate the change in array performance. The sensitivity of the characteristics of the individual slots to a given variation in slot dimensions is determined by using the slot design equations or design curves such as those shown in Fig. 4.

Systematic errors have more significant impacts. A consistent change in the waveguide a dimension shifts the resonant frequency of the standing-wave array and alters the beam-pointing angle in the traveling-wave array. A systematic error in the slot locations creates undesirable sidelobes. In the traveling-wave array, if the slot coupling or the waveguide losses are consistently higher or lower than the design value, the error in the array excitation accumulates along the array because the mode amplitude is increasingly perturbed. If the coupling is significantly lower than the design value, excess power is lost in the load. Periodic errors raise the sidelobe at the position where a grating lobe would occur for an array whose spacing is equal to the spacing of the periodic error. Feed-network or other errors that affect large portions of the array have significant impacts on the array sidelobe and gain performance. An array with a difference pattern requirement is sensitive to asymmetrical errors across the array because any imbalance affects the cancellation which occurs at the difference pattern null.

ACKNOWLEDGMENTS

The author wishes to thank W. H. Kummer for his assistance with the manuscript and historical background, R. C. Hansen for providing historical material, G. R. Kulakowski for his assistance with the figures and the reviewers for their helpful comments.

BIBLIOGRAPHY

1. G. C. Southworth, Hyper-frequency wave-guides—General considerations and experimental results, *Bell Syst. Tech J.,* **15**: 284–309, 1936.

2. J. R. Carson, S. M. Mead, and S. A. Schelkunoff, Hyper-frequency wave guides—Mathematical theory, *Bell Syst. Tech. J.,* **15**: 310–333, 1936.
3. W. L. Barrow, Transmission of electromagnetic waves in hollow tubes of metal, *Proc. IRE,* **24**: 1298–1398, 1936.
4. K. S. Packard, The origin of waveguides: A case of multiple rediscovery, *IEEE Trans. Microw. Theory Tech.,* **MTT-32**: 961–969, 1984.
5. S. A. Schelkunoff, The impedance concept and its application to problems of reflection, refraction, shielding, and power absorption, *Bell Syst. Tech. J.,* **17**: 17–48, 1938.
6. S. A. Schelkunoff, A mathematical theory of linear arrays, *Bell Syst. Tech. J.,* **22**: 80–107, 1943.
7. C. L. Dolph, A current distribution for broadside arrays which optimizes the relation between beamwidth and side lobe levels, *Proc. IRE,* **34**: 335–348, 1946.
8. T. T. Taylor, Design of line source antennas for narrow beamwidth and low sidelobe, *IRE Trans. Antennas Propag.,* **AP-7**: 15–28, 1955.
9. W. H. Watson, *The Physical Principles of Wave Guide Transmission and Antenna Systems,* Oxford, UK: Clarendon Press, 1947.
10. A. F. Stevenson, Theory of slots in rectangular waveguides, *J. Appl. Phys.,* **18**: 24–38, 1948.
11. S. Silver, *Microwave Antenna Theory and Design,* Vol. 12, MIT Rad Lab Series, New York: McGraw-Hill, 1949.
12. I. P. Kaminow and R. J. Stegen, *Waveguide slot array design,* Tech. Memo. No. 348, Hughes Aircraft Co. July 1954.
13. A. A. Oliner, The impedance properties of narrow radiating slots in the broad face of rectangular waveguide—Part I—theory, Part II—comparison with measurement, *IEEE Trans. Antennas Propag.,* **AP-5**: 4–20, 1957.
14. A. A. Oliner, Historical perspectives on microwave field theory, *IEEE Trans. Microw. Theory Tech.,* **MTT-32**: 1022–1045, 1984.
15. H. G. Booker, Slot aerials and their relations to complementary wire aerials (Babinet's principle), *J.I.E.E. (London),* **93, part IIIA**: 620–626, 1946.
16. Ref. 11, pp. 226–229.
17. R. S. Elliott, An improved design procedure for small arrays of shunt slots, *IEEE Trans. Antennas Propag.,* **AP-31**: 48–53, 1983.
18. Ref. 11, pp. 286–299.
19. R. F. Harrington, *Field Computation by Moment Methods,* New York: Macmillan, 1968.
20. V. T. Khac, A study of some slot discontinuities in rectangular waveguides, Ph.D. Dissertation, Monash Univ., Australia, Nov. 1974.
21. G. J. Stern and R. S. Elliott, Resonant length of longitudinal slots and validity of circuit representation: Theory and experiment, *IEEE Trans. Antennas Propag.,* **AP-33**: 1264–1271, 1985.
22. D. J. Lewis, *Waveguide Coulping Slots,* Internal memo., Hughes Aircraft Co.
23. S. R. Rengarajan, Analysis of a centered-inclined waveguide slot coupler, *IEEE Trans. Microw. Theory Tech.,* **37**: 884–889, 1989.
24. P. P. Silvester, *Finite Elements in Electrical and Magnetic Field Problems,* New York: Wiley, 1980.
25. J. L. Altman, *Microwave Circuits,* New York: Van Nostrand, 1964, pp. 399–406.
26. J. J. Gulick and R. S. Elliott, The design of linear and planar arrays of waveguide-fed longitudinal slots, *Electromagnetics,* **10** (4): 327–347, 1990.
27. R. S. Elliott, *Microwave Antenna Theory and Design,* Englewood Cliffs, NJ: Prentice-Hall, 1981.
28. N. A. Begovich, Frequency scanning, in R. C. Hansen (ed.), *Microwave Scanning Antennas,* Vol. 3, New York: Academic Press, 1964, Chap. 2.
29. R. S. Elliott, On the design of traveling-wave-fed longitudinal shunt slot arrays, *IEEE Trans. Antennas Propag.,* **AP-27**: 717–720, 1979.
30. E. O. Brigham, *The Fast Fourier Transform,* Englewood Cliffs, NJ: Prentice-Hall, 1974.
31. T. T. Taylor, Design of circular apertures for narrow beamwidth and low sidelobes, *IRE Trans. Antennas Propag.,* **8**: 17–22, 1960.
32. D. C. Senior, Higher order mode coupling effects in a shunt-series coulping junction in a planar slot array antenna, Ph.D. Dissertation, Univ. California at Los Angeles, 1986.
33. J. Ruze, The effects of aperture errors on the radiation pattern, *Nouvo Cimento,* **9** (Suppl. No. 3): 364–380, 1952.
34. R. S. Elliott, Mechanical and electrical tolerances for two-dimensional scanning antenna arrays, *IRE Trans. Antennas Propag.,* **10**: 114–120, 1958.

WINIFRED E. KUMMER
Raytheon Systems Company

WAVEGUIDE ATTENUATOR. See ATTENUATION MEASUREMENT; ATTENUATORS.

WAVEGUIDE CIRCUITS. See MICROWAVE CIRCUITS.

WAVEGUIDE FINLINES. See FINLINES.